Angewandte Chemie International Edition

DOI: 10.1002/anie.201103745

VIP High-Resolution Microscopy

Atomic-Scale Edge Structures on Industrial-Style MoS_2 Nanocatalysts**

*Lars P. Hansen, Quentin M. Ramasse, Christian Kisielowski, Michael Brorson, Erik Johnson, Henrik Topsøe, and Stig Helveg**

Dedicated to the Fritz Haber Institute, Berlin, on the occasion of its 100th anniversary

Currently, considerable interest is directed toward functional nanostructures, such as fullerenes, nanotubes/wires, and platelets, derived from molybdenum disulfide.[1] As platelets, MoS_2 is employed as catalyst for industrial oil refining, hydrogen evolution, and photooxidation.[2–5] The MoS_2 nanocatalyst basically consists of 2-dimensional S–Mo–S layers that are stacked to various degrees. The catalytic reactivity of the S–Mo–S layers is associated with their edges and detailed information about the edge structures is thus essential in order to understand the nature of the catalytically active sites.[6] Unprecedented atomic-scale insight into the MoS_2 edge structure and reactivity was obtained from scanning tunnelling microscopy (STM) of model catalysts, prepared under ultra-high-vacuum conditions on planar substrates, and from density functional theory (DFT) calculations. Such information has significantly improved the understanding of the structural-dependent catalytic properties[6] and may lead to further improvement in the formulation of the catalyst properties when combined with high-resolution electron microscopy of industrial-style MoS_2 nanocatalysts.[7–10]

Recently, unprecedented levels of imaging contrast and resolution became available due to advances in aberration-corrected high-resolution (scanning) transmission electron microscopy (HR(S)TEM)[11] and should benefit tremendously the study of edge structures on industrial-style MoS_2 nanocatalysts.[12] By HRTEM, we demonstrated that single-atom-sensitive images of industrial-style graphite-supported MoS_2 nanocatalysts, viewed in the (001) projection, may be obtained facilitating an unambiguous identification of single- and double-layer MoS_2 structures as well as a crystallographic indexation of the two predominant low-indexed edge types.[12] The detailed structural information was obtained from a phase image representing a reconstruction of a through-focus series of HRTEM images of the sample. However, due to edge reconstructions during the acquisition of the consecutive images, a determination of the atomic-scale structure of the catalytically important outermost edges was not directly possible. These edge reconstructions are most likely caused by knock-on damage induced by the incident electron beam (with a kinetic energy of 80 keV), whereas ionization damage is expected to be negligible due to the electrical conductivity of the sample. The knock-on damage may be reduced by lowering of the primary electron energy below its threshold energy,[13] which is approximately 66 keV for MoS_2 (see the Supporting Information). Only quite recently, HRSTEM under such conditions became possible.[14] Herein, we report HRSTEM images, acquired at low beam energy (60 keV), to obtain atomic-scale information about the edge structure of the industrial-style MoS_2 nanocatalysts and we compare the images with edge structures predicted by model catalyst studies and DFT calculations.

Figure 1 shows a HRSTEM image, acquired in the high-angle annular dark-field (HAADF) detection mode, of a nanometer-sized MoS_2 nanocrystal synthesized on a high-surface area graphitic support.[15] Consistent with our previous work, the nanocrystal has a slightly truncated triangular shape and a contrast pattern that reflects the structure of a MoS_2 lattice oriented with its (001) basal plane parallel to the graphite support and orthogonal to the electron beam.

To address the atomic arrangement in such a nanocrystal, the HRSTEM image intensities are analyzed in detail. Figure 2a shows a close-up of a MoS_2 nanocrystal and depicts the intensity levels associated with the graphite support and the MoS_2 nanocrystal. For the HAADF detection mode, the HRSTEM images are dominated by the so-called Z-contrast. In such images of zone-axis oriented crystalline materials, bright contrast coincides with atomic column positions and the intensity maxima scales with the total atomic number Z of the column roughly as $Z^{1.7}$.[16] Thus, the evaluation of the intensity distribution over the image in Figure 2a provides three-dimensional information about the support thickness and MoS_2 nanocrystal structure. As confirmed below, for the

---

[*] L. P. Hansen, M. Brorson, H. Topsøe, S. Helveg
Haldor Topsøe A/S
Nymøllevej 55, 2800 Kgs. Lyngby (Denmark)
E-mail: sth@topsoe.dk

Q. M. Ramasse
SuperSTEM Laboratory, STFC Daresbury
Keckwick Lane, Daresbury WA4 4AD (UK)

C. Kisielowski
Joint Center for Artificial Photosynthesis (JCAP), Lawrence Berkeley National Laboratory
1 Cyclotron Road, Berkeley, CA 94708 (USA)

E. Johnson
Nano-Science Center, Niels Bohr Institute
Universitetsparken 5, 2100 Copenhagen (Denmark)

[**] Microscopy was performed at the SuperSTEM Laboratory, Daresbury (UK). L.P.H. was financially supported by The Danish Council for Technology and Innovation (08-044837). The authors thank Berit Hinnemann and Burcin Temel (Haldor Topsøe A/S) for fruitful discussions.

Supporting information for this article is available on the WWW under http://dx.doi.org/10.1002/anie.201103745.

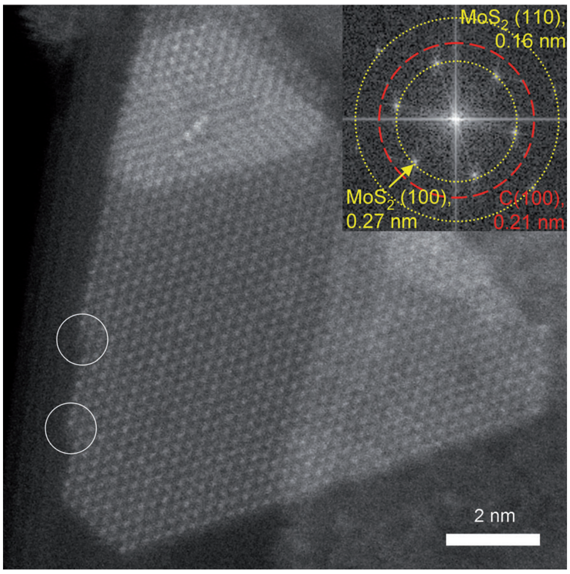

Figure 1. High-resolution STEM image of a MoS$_2$ nanocrystal supported on a graphite support. The insert is a fast Fourier transform (FFT) of the image and shows hexagonally arranged spots at the 0.27 nm and 0.16 nm lattice distances, corresponding to the MoS$_2$ (100) and (110) lattice planes, respectively. Moreover, a hexagonal set of lattice distances at 0.21 nm, corresponding to graphite (100), is also revealed. At the low-indexed edges, kink sites may be present as indicated by white circles.

stepped graphite support areas, Figure 2b shows intensity levels relative to the vacuum level that can be attributed to a graphite flake with a thickness of two (2C), three (3C), and four (4C) layers (see the Supporting Information). An additional carbon layer (5C) extending from the MoS$_2$ nanocrystal across the basal plane of the 4C layer can also be inferred. Figure 2a shows that the interior intensity pattern of the MoS$_2$ nanocrystal consists of a hexagonal arrangement of intensity maxima, with a separation of 0.18 nm that corresponds to the atomic columns of MoS$_2$ oriented with $\langle 001 \rangle$ along the electron beam direction. The maxima have an asymmetric intensity pattern (Figure 2b), thus suggesting that the chemical composition of each atomic column differs. The different intensity levels can be attributed to either a single Mo atom (Mo, $Z=42$) or two S atoms (2S, $Z=2\times 16$), so that the nanocrystal corresponds to a single-layer MoS$_2$. To confirm this element identification, Figure 2c shows that the relative intensities plotted versus the presumed element assignment is excellently described by a $Z^{1.74}$-dependency, in accordance with Hartel et al.[16] It should be noted that other combinations of elements (such as different multiples of C layers: 4C, 6C, and 8C, for instance, or of odd multiples of MoS$_2$ layers) did not match the expected $Z^{1.7}$-dependent intensity distribution.

Based on the element identification in the basal plane, the crystallographic identity of the various edges of the MoS$_2$ nanocrystal can be inferred.[12] Specifically, the longer edges can be assigned as (100) Mo edges and the shorter edges as $(\bar{1}00)$ S edges. Along the Mo edges, Figure 2a reveals bright features with a periodicity corresponding to the S separation along (100) and with an intensity level less than the 2S

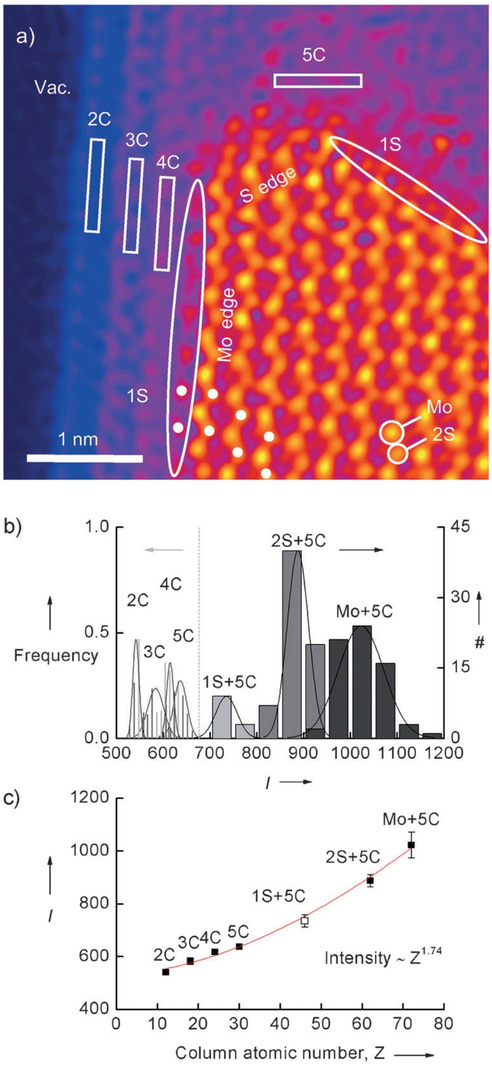

Figure 2. a) High-resolution STEM image of a single-layer MoS$_2$ nanocrystal on a graphite support oriented with the MoS$_2$ $\langle 001 \rangle$ direction along the electron beam. The image intensity contributions from the tail of the scanning electron probe on the neighboring atomic columns, as well as the noise in the image, were reduced by a probe deconvolution using a maximum entropy algorithm (see the Supporting Information).[17] Moreover, the image is colorized to further improve the visibility of the different intensity levels. White dots superimposed the image denote sulfur sublattice positions of the MoS$_2$ basal plane and Mo edge. b) Left-hand scale: Histograms (shown with best Gaussian fits) of intensity (I) level from line-profiles of the graphite areas as indicated with rectangular boxes (2C-5C) in Figure 2a. The intensity line profiles were averaged over the width of the boxes corresponding to the estimated probe size (0.11 nm). Right-hand scale: Distributions of peak intensities at atomic column positions in the MoS$_2$ nanocrystal. The peak intensities were obtained from line scans manually adjusted to $\langle 100 \rangle$ and averaged over a width corresponding to the estimated probe size (0.11 nm). Fitted Gaussian profiles (black lines) are shown to ease comparison with the intensity distribution in the graphite areas. c) The average intensities of the distributions in Figure 2b as a function of the assigned total atomic number Z of the atomic column. The error bars denote the standard deviations of the intensity distributions. The best power function fit (red line), disregarding the vacuum level (Vac.) and Mo-edge termination (open symbol), is obtained with $I\approx Z^{1.74}$. The vacuum level differed from zero intensity as the detector amplification and black levels were set intentionally high to avoid clipping of low-contrast features.

columns (see Figure 2a). Based on Figure 2c, the average maximum intensity of these features corresponds exactly to a column that contains one S atom on the 5C support (i.e. a 1S+5C column). That is, the Mo-edge appears to be terminated by single sulfur atoms. It should be emphasized that the curve in Figure 2c was fitted without the use of these 1S+5C datapoints. From a closer inspection of the images, the registry of the 1S atomic columns relative to the 2S columns in the basal plane of MoS_2 can be determined (indicated by white dots, Figure 2a). Figure 2a and 3a show that the 1S columns are shifted by half a lattice constant along the Mo edge and thus are out of registry with the hexagonal sublattice of the 2S columns in the MoS_2 basal plane. Thus, the images of these industrial-style MoS_2 nanocatalysts show that the Mo edge is not just a simple truncation of the bulk MoS_2 structure, which is an observation consistent with the DFT and STM studies.[18–23]

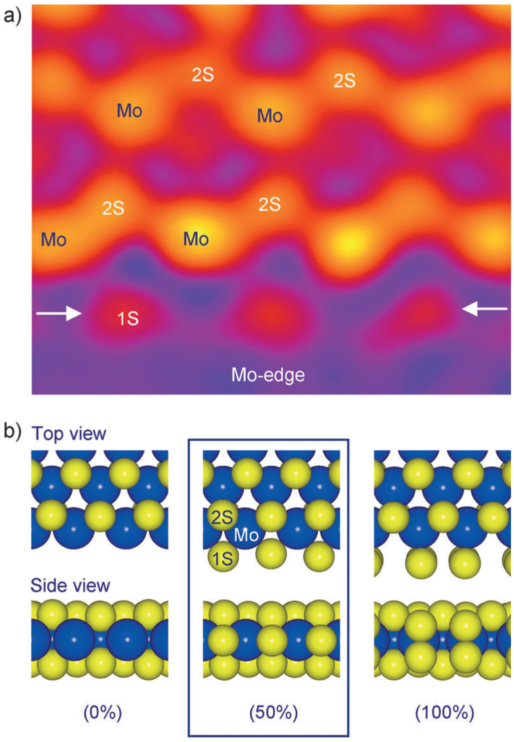

Figure 3. Detailed atomic structure analysis of part of a single-layer MoS_2 nanocrystal in (001) projection on graphite support (Figure 2a). a) High-resolution STEM image, which is probe-deconvoluted and colorized for improved visibility. The arrows point to single sulfur atoms that terminate the Mo edge as designated by an intensity analysis. b) Ball models (top and side views, respectively) of different S coverage levels at the Mo edge (0%, 50%, 100%), adapted from [20].

Experimental STM and theoretical DFT studies have shown that depending on synthesis and imaging conditions, different sulfur termination structures are possible for the Mo (and S) edges of single-layer MoS_2.[18–23] Figure 3b shows ball models of such possible Mo edge structures. Herein, the bare Mo edge termination (0% S coverage) consists of undercoordinated Mo atoms with each Mo bonded to only four sulfur atoms. Under catalyst sulfiding conditions, the edge termination at 0% sulfur coverage is considered very unfavorable relative to the Mo edge terminations with a 50% or 100% sulfur coverage for which Mo can achieve a full sixfold coordination by sulfur.[20–23] The Mo edge with 50% sulfur coverage is severely reconstructed with terminating sulfur atoms shifted laterally by half a lattice constant with respect to the sulfur sublattice in the MoS_2 basal plane and vertically to positions in-plane with the Mo sublattice (Figure 3b). For the fully sulfided (100%) Mo edge, the edge is expected to be terminated by sulfur "dimers" (with a slight pairing in the 001 direction)[20] that are located in registry with the sulfur sublattice at the MoS_2 basal plane. Thus, the present HRSTEM observations of a Mo edge termination with single S atoms on an industrial-style MoS_2 nanocatalyst match the 50% sulfur covered Mo edge structure of the model studies.

Occasionally, during the sequential image acquisition, creation of point defects along the Mo edge was also observed, which is indicative of the onset of beam knock-on damage. At the S edge, the irregular atom configuration is attributed to a similar but more pronounced beam effect. However, pristine HRSTEM images of the rather short S edge appear to be consistent with the model predictions for an S edge of at least 50% S coverage (see the Supporting Information). The observed lower stability of the S edge compared to the Mo edge may be due to the difference in edge energy or due to corners, as the S edge was short.[23]

The expected Mo edge termination structure can be determined by a thermodynamic extension of the DFT results[19,21–23] to the present sulfiding conditions. Following Bollinger et al.,[22] the relative stability of various edge terminations for an (unsupported) single-layer MoS_2 structure depends on the (relative) chemical potentials of sulfur, $\mu_S - \mu_{S(bulk)}$ and hydrogen, $\mu_H - 1/2\,E_{H2}$. As a function of these chemical potentials, the more stable edge terminations can be expressed by means of a phase diagram. The present sulfiding conditions, that is, the partial pressures of H_2 and H_2S ($p_{H2} = 0.9$ bar, $p_{H2S} = 0.1$ bar, respectively) and the sulfidation temperature ($T = 1073$ K), are described by $\mu_S - \mu_{S(bulk)} = -1.28$ eV and $\mu_H - 1/2\,E_{H2} = -0.64$ eV. In the same gas mixture at room temperature ($T = 300$ K), $\mu_S - \mu_{S(bulk)} = -0.49$ eV and $\mu_H - 1/2\,E_{H2} = -0.024$ eV. For both sets of conditions, the phase diagram clearly predicts a 50% sulfur covered Mo edge, with S atoms arranged in the reconstructed geometry as the more stable termination.[18,22] That is, the prediction made by the model catalyst studies is consistent with the present HRSTEM observations of the industrial-style nanocatalyst in an inert environment at room temperature. In fact, at room temperature, DFT predicts that the stable Mo edge termination includes adsorbed hydrogen atoms[18,22] that unfortunately are undetectable in the present images.

Previously, experimental information about the MoS_2 edge terminations was accessed through model catalysts prepared under high-vacuum conditions with planar, single-crystalline supports by STM. Thus, it has remained to be addressed whether information from the model studies indeed can be related to the industrial-style nanocatalysts. This problem has been referred to as "the materials gap" in the field of catalysis. The present MoS_2 nanocatalyst differs significantly from the previous model systems as it employs a high-surface area support and a wet impregnation preparation as in industrial catalysts. Specifically, the present results show that it is indeed possible to obtain direct atomic structure information about the catalytically important edges of industrially relevant MoS_2 nanocatalysts, which is not available from STM. Moreover, the observed low-indexed edge structures are not only consistent with the previous experimental and theoretical model studies but also reveal the presence of corners and kink sites (Figure 1). Although the reactivity of corner sites was considered in model studies,[24] the role of kink sites has not previously been considered. As the kinks represent joints between Mo and S edges with a concave geometry, such sites may provide a favorable bonding geometry to mediate the dual functionality of the adjacent edges[25] toward a combined hydrogenation and desulfurization reaction step. Further interplay with STM and DFT may examine such site-specific reactivity in detail.

Experimental Section

The industrial-style (cobalt-promoted) MoS_2 hydrotreating catalyst was prepared by incipient wetness impregnation of a high-surface area graphitic carbon support according to Brorson et al.[15] After sulfidation at $T = 1073$ K, the sample was cooled to room temperature (300 K) in the sulfiding gas. The sulfiding gas was then replaced by inert, dry N_2 under which the MoS_2 nanocrystals are expected to remain stable at room temperature. For electron microscopy analyses, the catalyst powder was crushed in a mortar and dispersed dry onto holey carbon films on a TEM Cu grid in dry O_2-free environment. The samples were kept and transported in O_2-free atmospheres at room temperature and only exposed to ambient conditions for a few minutes during sample loading into the microscope.

All electron microscopy was carried out on a Nion UltraSTEM 100 aberration-corrected dedicated scanning transmission electron microscope (STEM). The instrument is equipped with a cold field emission electron gun, with a native energy spread of 0.35 eV, and was operated with a primary electron energy of 60 keV in order to minimize sample damage. The beam was set up to a convergence semi-angle of 28 mrad and an estimated beam current of 40 pA at the sample. At these operating conditions, the estimated probe size was 1.1 Å. The images were acquired in high angle annular dark field (HAADF) mode with the inner and outer detector radii being calibrated at 95 mrad and 190 mrad, respectively. Although at 60 keV primary energy the effect of knock-on damage on the sample is drastically reduced, the beam dwell times were kept relatively short in order to minimize the total electron dose and the imaging conditions (fine focus and astigmatism corrections) were fine-tuned slightly away from the particles of interest before moving them into the field of view to acquire images shown here.

Received: June 1, 2011

Keywords: chalcogens · electron microscopy · heterogeneous catalysis · molybdenum disulfide · single-atom imaging

---

[1] R. Tenne, *Angew. Chem.* **2003**, *115*, 5280–5289; *Angew. Chem. Int. Ed.* **2003**, *42*, 5124–5132; R. Tenne, *Nat. Nanotechnol.* **2006**, *1*, 103–111.

[2] R. Prins, *Adv. Catal.* **2001**, *46*, 399–464.

[3] T. F. Jaramillo, K. P. Jørgensen, J. Bonde, J. H. Nielsen, S. Horch, I. Chorkendorff, *Science* **2007**, *317*, 100–102.

[4] Y. Li, H. Wang, L. Xie, Y. Liang, G. Hong, H. Dai, *J. Am. Chem. Soc.* **2011**, *133*, 7296–7299.

[5] J. P. Wilcoxon, T. R. Thurston, J. E. Martin, *Nanostruct. Mater.* **1999**, *12*, 993–997.

[6] F. Besenbacher, M. Brorson, B. S. Clausen, S. Helveg, B. Hinnemann, J. Kibsgaard, J. V. Lauritsen, P. G. Moses, J. K. Nørskov, H. Topsøe, *Catal. Today* **2008**, *130*, 86–96.

[7] K. P. de Jong, L. C. A. van den Oetelaar, E. T. C. Vogt, S. Eijsbouts, A. J. Koster, H. Friedrich, P. E. de Jongh, *J. Phys. Chem. B* **2006**, *110*, 10209–10212.

[8] E. J. M. Hensen, P. J. Kooymann, Y. van der Meer, A. M. van der Kraan, V. H. J. de Beer, J. A. R. van Veen, R. A. van Santen, *J. Catal.* **2001**, *199*, 224–235.

[9] R. M. Stockmann, H. W. Zandbergen, A. D. van Langeveld, J. A. Moulijn, *J. Mol. Catal. A* **1995**, *102*, 147–161.

[10] F. L. Deepak, R. Esparza, B. Borges, X. López-Lozano, M. José-Yacamán, *Catal. Lett.* **2011**, *141*, 518–524.

[11] a) C. Girit, et al., *Science* **2009**, *323*, 1705–1708; see Supporting Information; b) Z. Y. Li, N. P. Young, M. Di Vece, S. Palomba, R. E. Palmer, A. L. Bleloch, B. C. Curley, R. L. Johnston, J. Jiang, J. Yuan, *Nature* **2008**, *451*, 46–49; c) L. C. Gontard, L.-Y. Chang, C. J. D. Hetherington, A. I. Kirkland, D. Ozkaya, R. E. Dunin-Borkowski, *Angew. Chem.* **2007**, *119*, 3757–3759; *Angew. Chem. Int. Ed.* **2007**, *46*, 3683–3685.

[12] C. Kisielowski, Q. M. Ramasse, L. P. Hansen, M. Brorson, A. Carlsson, A. M. Molenbroeck, H. Topsøe, S. Helveg, *Angew. Chem.* **2010**, *122*, 2768–2770; *Angew. Chem. Int. Ed.* **2010**, *49*, 2708–2710.

[13] R. F. Egerton, R. McLeod, F. Wang, M. Malac, *Ultramicroscopy* **2010**, *110*, 991–997.

[14] a) R. Zan, U. Bangert, Q. M. Ramasse, K. S. Novoselov, *Nano Lett.* **2011**, *11*, 1087–1092; b) O. L. Krivanek, et al., *Nature* **2010**, *464*, 571–575; see Supporting Information; c) Z. Liu, K. Suenaga, Z. Wang, Z. Shi, E. Okunishi, S. Iijima, *Nat. Commun.* **2011**, *2*, 1–5.

[15] M. Brorson, A. Carlsson, H. Topsøe, *Catal. Today* **2007**, *123*, 31-36.

[16] P. Hartel, H. Rose, C. Dinges, *Ultramicroscopy* **1996**, *63*, 93–114.

[17] K. Ishizuka, E. Abe, *Proc. of the 13th European Microscopy Congress, Instrumentation and Methodology* **2004**, *1*, 117. DeconvHAADF is available commercially from HREM Research Inc. (www.hremresearch.com).

[18] J. V. Lauritsen, M. V. Bollinger, E. Lægsgaard, K. W. Jacobsen, J. K. Nørskov, B. S. Clausen, H. Topsøe, F. Besenbacher, *J. Catal.* **2004**, *221*, 510–522.

[19] S. Cristol, J. F. Paul, E. Payen, D. Bougeard, S. Clémendot, F. Hutschka, *J. Phys. Chem. B* **2000**, *104*, 11220–11229.

[20] L. S. Byskov, J. K. Nørskov, B. S. Clausen, H. Topsøe, *J. Catal.* **1999**, *187*, 109–122.

[21] H. Schweiger, P. Raybaud, G. Kresse, H. Toulhoat, *J. Catal.* **2002**, *207*, 76–87.

[22] M. V. Bollinger, K. W. Jacobsen, J. K. Nørskov, *Phys. Rev. B* **2003**, *67*, 085410.

[23] P.-Y. Prodhomme, P. Raybaud, H. Toulhoat, *J. Catal.* **2011**, *280*, 178–195.

[24] A. Tuxen, J. Kibsgaard, H. Gøbel, E. Lægsgaard, H. Topsøe, J. V. Lauritsen, F. Besenbacher, *ACS Nano* **2010**, *4*, 4677–4682.

[25] P. G. Moses, B. Hinnemann, H. Topsøe, J. K. Nørskov, *J. Catal.* **2007**, *248*, 188–203.